CHEMISTRY OF MATERIALS

ARTICLE

pubs.acs.org/cm

$NbVO_5$ Mesoporous Thin Films by Evaporation Induced Micelles Packing: Pore Size Dependence of the Mechanical Stability upon Thermal Treatment and Li Insertion/Extraction

Natacha Krins,[†,‡] John D. Bass,[‡] David Grosso,[‡] Catherine Henrist,[†] Romain Delaigle,[§] Eric M. Gaigneaux,[§] Rudi Cloots,[†] Bénédicte Vertruyen,[†] and Clément Sanchez*[,‡]

[†]LCIS-GreenMat, Chemistry Institute B6, University of Liège, B-4000 Liège (Sart-Tilman), Belgium

[‡]Chimie de la Matière Condensée de Paris, UMR UPMC-CNRS 7574, Université Pierre et Marie Curie (Paris 6), Collège de France, 11 place Marcelin Berthelot, 75231 Paris, France

[§]Université Catholique de Louvain, Institute of Condensed Matter and Nanosciences, Division Molecules Solids and Reactivity, Croix du Sud 2/17, B-1348 Louvain-la-Neuve, Belgium

Supporting Information

ABSTRACT: Mesoporous thin films (MTFs) appear as an interesting architecture for positive electrodes in Li-ion energy storage systems because they offer high specific area and interconnected porosity presenting homogeneous pore size and wall thickness. However, it must be ascertained that the mesostructure survives template removal or/and crystallization and is retained on electrochemical cycling. In order to investigate the potentialities and limits of the soft-templating approach in the case of complex transition metal oxide networks, we deliberately selected a "difficult" compound: $NbVO_5$ was chosen because it combines a challenging synthesis with reported severe structural distortions during the first lithium insertion in the bulk material. In this work, $NbVO_5$ MTFs with different pore sizes were synthesized using the evaporation induced micelles packing (EIMP) method. PS-*b*-PEO diblock copolymers of different molar weights were used as structure directing agent in order to obtain wormlike porous networks with pore size and wall thickness ranging from 15 to 100 nm. Thermal ellipsometry analysis, used to track surfactant removal and crystallization of the layer, reveals that partial crystallization is possible while retaining the mesoporous architecture. Electron tomography complements result from environmental ellipsometric porosimetry, atomic force microscopy, and transmission electron microscopy to provide a comprehensive description of the structure. A multilayer process is also proposed to build crack-free thick mesoporous films. The mechanical stability of MTFs presenting three different pore sizes is tested by inserting Li^+ in amorphous $NbVO_5$ MTFs using cyclic voltammetry. Capacity retention data show that the mechanical stresses associated with Li^+ insertion are better accommodated by MTFs compared to nonporous films, and this ability is enhanced as the pore size decreases.

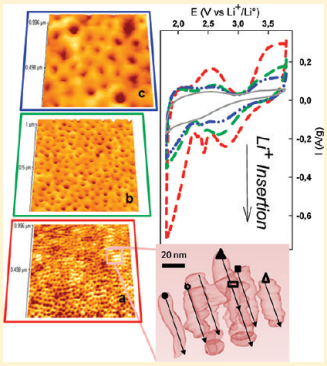

KEYWORDS: mesoporous thin film, $NbVO_5$, Li battery, self-assembling, in situ thermal ellipsometry analysis, cyclic voltammetry, electron tomography

1. INTRODUCTION

Mesoporous thin films (MTFs) have recently attracted a lot of interest in the field of energy storage in high power devices.[1−6] In lithium batteries or electrochemical capacitors, the "nano" effect enables shorter diffusions paths for both lithium ion and electrons, facilitating their transport and a higher lithium flux across the interface.[7−10] MTFs, in particular, present a large surface area and interconnected porosity which enables an excellent accessibility of the electrolyte to the inner surface (1).[11] If the MTF network turns out to be mechanically robust and able to support cycling, this architecture should not suffer from the loss of electrical contact encountered in nanoparticle electrodes as a result of the volume expansions experienced during the intercalation/deintercalation reactions. In addition, as no extra conducting and binding reagents are added to the electrode, MTFs are ideal models for understanding how the structural parameters influence the electrochemical performance.[12,13]

In order to investigate the potentialities and limits of the soft-templating approach in the case of complex oxide MTFs, this work takes the challenge of synthesizing a metastable bicationic oxide, $NbVO_5$, as mesoporous thin films with different pore sizes using a structure directing self-assembling method.

In the early 1990s, bulk $NbVO_5$ has been investigated as an electrode candidate in lithium batteries because it presents two types of channels available for lithium ions transport; however, it turned out to present a large structural distortion upon lithium

Received: December 6, 2010
Revised: July 27, 2011
Published: August 30, 2011

intercalation which causes 90% loss of capacity after the first cycle.[14,15] The distortion occurring upon the first Li^+ intercalation is attributed to the fact that, in the $NbVO_5$ structure, V^{5+} occupies tetrahedral sites. These sites are too small to accommodate the V^{4+} species formed after Li^+ intercalation, leading to a deformation of the oxygen network and consequently to the trapping of Li^+ species inside the framework.[16] In a recent work, Ren et al.[17,18] have shown that mesopores (between 10 and 100 nm) in β-MnO_2 micrometer-sized particles act as a buffer to alleviate the adverse effect of volume expansion through elastic deformation, thereby improving the cycling behavior. We here propose to test the $NbVO_5$ MTFs to investigate to which extent a mesoporous thin film architecture, depending on the pore size (from 15 to 100 nm), can help to accommodate significant stresses.

The synthesis of MTFs of several transition metal oxides can be achieved relatively easily by techniques combining sol−gel and evaporation induced self-assembly (EISA) of a block copolymer with complexation of molecular inorganic species.[11] However, it remains quite challenging to prepare vanadium oxide MTFs due to the lack of thermal stability.[19,20] This results from the complexity of the vanadium chemistry in terms of valence and coordination states, added to the fact that the condensation reactions of the oxide network might be incomplete.[21,22]

In 2005, Yuan et al.[23] obtained mixed MTFs of Nb−V oxides (70−30 mol %) by EISA. In order to increase the vanadium content to 50% or more, a structuring agent of high thermal stability is necessary: the possibility to use higher temperature should promote a more complete condensation of the inorganic network. Sallard et al.[13] have used such an approach to obtain MTFs of WO_3 with a KLE (poly(ethylene-co-butylene)-*b*-poly(ethylene oxide)) amphiphilic surfactant.

In a preliminary study of the $Nb_{2x}V_{2-2x}O_5$ ($0 \leq x \leq 1$) system,[24] we empirically found that a 50−50 mol % mesoporous architecture could be obtained using another amphiphilic diblock copolymer surfactant: polystyrene-*b*-polyethylene (PS-*b*-PEO), whose PS part is known to be calcined at high temperature.[25,26] We preliminarly checked by cyclic voltammetry that lithium may be inserted/deinserted in these MTFs, with an electrochemical capacity higher than that of a nonporous thin film of the same composition.[24] These first results suggested that $NbVO_5$ was a promising phase for our study.

In the present paper, we use in situ thermal ellipsometric analysis to elucidate the thermal behavior of the surfactant-mixed oxide hybrid thin films for three molar weights of the PS-*b*-PEO surfactant. This technique gives access to the pyrolysis temperature of the surfactant and the crystallization temperature of the inorganic walls. Based on these results, we discuss the influence of the surfactant size on the formation of amorphous/crystalline $NbVO_5$ MTFs, showing that only partial crystallization of $NbVO_5$ MTFs could be achieved. However, amorphous MTFs heated just below the crystallization limit present characteristics reminiscent of the crystalline phase: vanadium in the +5 oxidation state and tetrahedral coordination, as confirmed by several structural characterizations (electron paramagnetic resonance, X-ray photoelectron spectroscopy, and ^{51}V nuclear magnetic resonance). They are therefore expected to suffer from the large structural distortion induced by the first lithium insertion, as required to test the stability of the MTF architecture against significant mechanical stresses. Lithium insertion−extraction in MTFs with different pore sizes and nonporous films was carried out by cyclic voltammetry.

Electron tomography in the transmission electron microscope (TEM-TOMO) was combined with atomic force microscopy, transmission electron microscopy, and environmental ellipsometry porosimetry to reach a comprehensive description of the porous amorphous $NbVO_5$ network. The pore shape and their 3D interconnectivity can be visualized through a movie included in the paper. We also propose a process to achieve crackfree thick MTFs (up to 1.3 μm) through a multilayer deposition process taking advantage of the use of a thermally stable structuring agent.

2. EXPERIMENTAL SECTION

2.1. Film Preparation. Mesoporous thin films of $NbVO_5$ were prepared by the evaporation-induced micelles packing method (EIMP).[27] Three polystyrene-*block*-polyethyleneoxide (PS-*b*-PEO) structuring agents were used. The molecular weights of the PS and PEO blocks in hereafter-named PSA, PSB, and PSC surfactants are 17,000 g/mol and 39,000 g/mol (PSA), 40,000 g/mol and 110,000 g/mol (PSB), and 105,000 g/mol and 190,000 g/mol (PSC). In a typical synthesis, 100 mg of surfactant (PSA/PSB/PSC) is dissolved in 1.4 g of tetrahydrofuran (THF) and heated a few minutes at 70 °C in order to achieve complete dissolution. After cooling, 1.5 g of ethanol, 2 mL of a $NbCl_5$ solution (0.9 mol·L^{-1} in ethanol), and 2 mL of a VCl_4 solution (0.9 mol·L^{-1} in ethanol) are added. The solution is then equilibrated for 1 h before adding 0.32 g of distilled H_2O. The as obtained blue-green solution is kept one night at 10 °C and is finally heated successively 3 times at 70 °C for 1 min just before dip coating. The substrate (superficially oxidized silicon wafer, FTO-coated glass, or 0.14-mm-thick glass) is dipped in the solution and withdrawn at a rate of 1−2.5 mm/s at a relative humidity of 10%. The film is then stabilized at 180 °C for 10 min in air. Multilayer films are obtained by repeating the procedure several times. The single-layer and multilayer films are then calcined at 350 °C for 10 min and finally annealed at 500 °C for 1 min in air. A single layer film is typically 100-nm thick.

Dense films were also prepared in the same conditions but without PS-*b*-PEO surfactants. Wettability of the substrate was improved by adding ~1 mg of F127 (EO_{100}-PO_{65}-EO_{100}) to these solutions.

Metallic-free PSA/PSB/PSC based solutions were also prepared for diffusion light scattering measurements following the previously described procedure except that 4 mL of ethanol was added in place of 4 mL of the vanadium/niobium chloride precursor solution.

2.2. Characterization. Dynamic light scattering measurements were performed using Viscotek 802 DLS. Atomic force microscopy (AFM) was performed with a Veeco DI-CPII in noncontact mode. Scanning electron microscopy (SEM) was performed using a Philips XL30 FEG-SEM. Transmission electron micrographs (TEM) of fragments scratched from the films were obtained in a TECNAI G2 TWIN (LaB_6, 200 kV). An electron tomogram was recorded thanks to the *Suite Explore 3D* (from *FEI Company*). The sample was tilted from −60° to +60°, with a 1.5° step. The treatment of the TEM images to obtain the reconstructed volume and the isosurfaces was done with the program *Amirar* (from *Mercury*).

Ellipsometry measurements were performed on a UV−visible (240−1000 nm) variable angle spectroscopic ellipsometer from Woollam and analyzed with the WVase32 software. Environmental ellipsometry porosimetry measurements were conducted using a controlled relative humidity chamber at room temperature. Pore volumes and pore size distributions were obtained from the film refractive index and thickness data using the isotropic inorganic pore contraction model (IIC) and a modified Kelvin equation.[28] Thermal ellipsometric analyses (TEA) were performed at 10 °C/min using a previously described setup.[29] X-ray diffractograms were obtained using a Bruker D8 grazing incidence diffractometer (Cu Kα radiation, 1° incidence, 0.04°/s step size, 3 s/step).

dx.doi.org/10.1021/cm103481n |*Chem. Mater.* 2011, 23, 4124–4131

^{51}V static NMR patterns were recorded on scratched and ground films mixed with SiO_2 in a Bruker Avance DSX 400WB spectrometer (B_0 = 9.04 T, pulse width = 0.8 μs; delay time = 0.2 s). The chemical shifts were referenced relative to Na_3VO_4. EPR measurements were recorded at 10 K in a Bruker Elexsys-500 spectrometer (X band; ν = 9.3813 GHz) on films deposited on thin glass and ground to powder. The simulation and numerical double integration of the spectra (see Figure S.I.4 of the Supporting Information for details) were performed using EasySpin.[30] XPS analyses (C 1s, O 1s, V 2p, K 2p, Nb 3d) were performed on a Kratos Axis Ultra spectrometer (Kratos Analytical, Manchester, U.K.) equipped with a monochromatized aluminum X-ray source (powered at 10 mA and 15 kV). Special care was taken to avoid vanadium reduction under vacuum.[31] A detailed description is provided in Figure S.I.4 of the Supporting Information.

Electrochemical tests were performed using a conventional cell. Two Li foils were used as negative and reference electrodes; the film (deposited on FTO/glass substrates) was used as positive electrode (area = 4 cm^2). The electrolyte was 1 $mol \cdot L^{-1}$ $LiPF_6$ in ethylene carbonate/dimethyl carbonate (1/1 v/v). Cyclic voltammograms were measured using a PAR 263A potentiostat from 3.8 to 1.8 V vs $Li^+/Li°$ at various scan rates (0.007, 0.05, 0.1, 0.5, 1, 5, 20, 50, and 100 mV/s). The negative current corresponds to reduction processes. The effective active mass of the electrode can be deduced from the thickness and the porosity obtained from ellipsometric measurements.

3. RESULTS AND DISCUSSION

3.1. Solution Characterization. Prior to chemical solution deposition (CSD), diffusion light scattering (DLS) measurements were performed in order to probe a possible organization of the structuring agent. In metal-free PSA, PSB, and PSC solutions, micelles are present and exhibit a narrow diameter size distribution centered at 20, 60, and 100 nm, respectively (see Figure S.I.1 of the Supporting Information). In the corresponding solutions containing V and Nb precursors, the micelle sizes increase to 40, 100, and 350 nm, respectively (see Figure S.I.1 of the Supporting Information). Since the surfactant concentration was kept constant (see the Experimental Section), the increase of the micelle apparent diameter highlights the chelating role of PEO with respect to the inorganic species.[32] Besides, the presence of micelles indicates that the formation of hybrid films by CSD results from an evaporation induced micelles packing process (EIMP), preferentially to the well-known evaporation induced self-assembly (EISA) procedure.[27]

3.2. From Hybrid Films to MTFs. Going from hybrid films to crystalline mesoporous films requires a finely tuned thermal treatment. In order to throw some light on the temperature range of the removal of the template and the crystallization of the vanadium niobium mixed oxide, the behavior of the hybrid films was followed *in situ* while heating by thermal ellipsometric analysis (TEA).[29] As an illustration, the variations of the thickness and the refractive index of PSB-based hybrid film are reported in Figure 1. The corresponding derivative curves are also shown in Figure 1. The data for PSA- and PSC-hybrid films are shown in the Supporting Information (Figure S.I.2).

The derivative curve of the refractive index presents three maxima, corresponding to three main processes (denoted I, II, and III in Figure 1) occurring during the thermal treatment.

Process I is described by a large contraction and a rapid increase of the refractive index of the film, suggesting a significant densification of the inorganic walls allowed by the removal of the PEO shell part of the micelles. Process II is characterized by a large drop in the refractive index, which means that porosity is

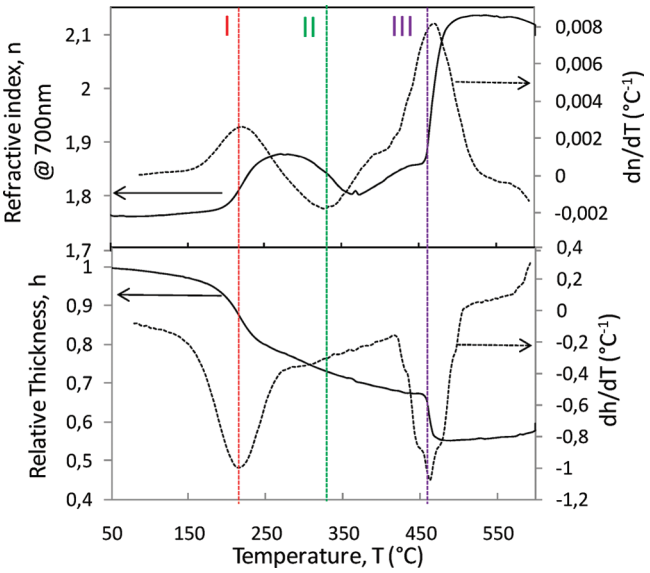

Figure 1. Thermal ellipsometric analysis collected at a ramp of 10 °C/min. Temperature dependence of the refractive index (top) and the relative thickness (bottom) for $NbVO_5$ PSB-film and the corresponding derivatives of the curves (dashed lines).

generated after the removal of the PS core. Simultaneously, the thickness decreases because of the thermally induced unidirectional contraction of the porous network, already reported for other oxide systems.[33]

From the TEA results obtained for the PSA, PSB, and PSC hybrid films, it is deduced that the temperature range of template departure (process I + II) slightly depends on the copolymer size. It is equal to 180−350 °C for PSA, 200−360 °C for PSB, and 200−390 °C for PSC.

Process III is characterized by an abrupt decrease in the relative thickness together with a drastic increase in the refractive index. This corresponds to a rapid and large densification of the film resulting from the destruction of the porous framework. Such a collapse of the mesostructure at high temperature could be due to the fact that the porous network cannot sustain the extensive diffusive sintering process which follows the formation of crystallites in the inorganic walls. The temperature of process III depends significantly on the surfactant size; it is evaluated to be 440, 460, and 465 °C for PSA-, PSB-, and PSC-based films. The high slope of the increase in the refractive index curve and the associated decrease in the film thickness suggest that process III is very fast.

To confirm that process III is correctly ascribed to the collapse of the mesoporous structure after crystallization of $NbVO_5$, *ex-situ* TEM images of PSB-films treated to 430 and 465 °C are shown in Figure 2d and e, respectively. Figure 2d shows a well-defined wormlike mesoporous network. However, in the case of the treatment at a slightly higher temperature (Figure 2e), the mesoporous network seems to be partially collapsed and the diffraction pattern indicates the presence of crystallites inside the inorganic walls. The same study was conducted for PSA films, and the results are presented in Figure 2a and b. It appears that the collapse of the mesostructure is already observed at 445 °C. Crystallites are detected on the diffraction pattern and are highlighted by bright spots in the corresponding dark-field image (Figure 2c). Since the $NbVO_5$ crystallization temperature is not pore size dependent (T_{cryst} = 440 °C) and since the

dx.doi.org/10.1021/cm103481n |*Chem. Mater.* 2011, 23, 4124–4131

temperature of the mesostructure collapse (process III) increases from PSA- to PSC-based films, it is deduced that mesoarchitecture presenting thicker walls (typically PSB and PSC) is able to better accommodate diffusive sintering and, therefore, to enclose $NbVO_5$ small crystallites. This behavior has already been reported in the literature for other transition metal oxides.[20,34,35]

Thermal ellipsometric analysis has shown that a fine-tuning of the thermal treatment was of utmost importance in order to preserve the mesoporous network. On the basis of the TEA curves, an efficient short heat treatment was developed to obtain mesoporous niobium vanadium mixed oxide films from the hybrid films. The films were first treated at 350 °C for 10 min in order to condense the inorganic mixed oxide network, while removing most of the organic part. A short treatment at a higher temperature (1 min at 500 °C) was then applied to strengthen the inorganic framework, to eliminate the last residues of surfactant. X-ray diffraction confirmed that the amorphous character was retained, as shown in Figure S.I.3(a) of the Supporting Information. It has to be noted that 500 °C is higher than the temperature of process III deduced from TEA; however, a film heated progressively to 450 °C and one flashed at 500 °C for 1 min have different thermal histories and, thus, different energy inputs, which can explain why a film flashed at 500 °C is still amorphous.

3.3. Characterization of MTFs. The PSA, PSB, and PSC films heated at 500 °C for 1 min were investigated by TEM and AFM (Figure 3).

A porous architecture appears to be successfully achieved whatever the structuring agent. The pore size increases when the size of the copolymer blocks increases. Typical pore sizes are ~15, ~50, and ~100 nm (macroporous) for PSA, PSB, and PSC films, respectively. The pore size distribution is quite narrow for PSA and PSB films; however, it is quite large for the PSC film even though the micelle size distribution was narrow in the solution. The thickness of the inorganic walls is in the same size range as the pore size. The increased pore size (from PSA to PSC) is related to the larger effective size of the micelles, while the increased thickness of the inorganic walls is related to the increasing molar ratio between M_T and PS-PEO (M_T/PS-PEO).[11] In the case of PSA and PSB films, the pores appear to be wormlike structured.

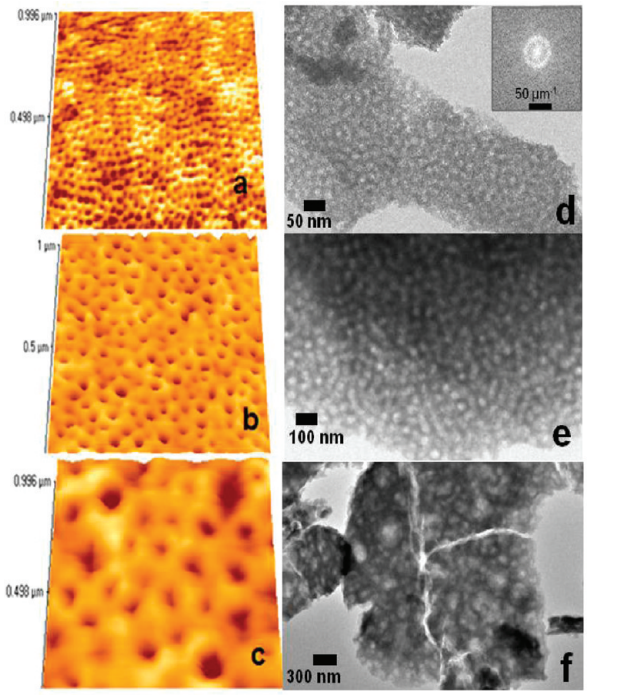

Figure 3. AFM (a, b, c) and TEM (d, e, f) images of amorphous $NbVO_5$ MTFs prepared by EIMP using (a, d) PSA, (b, e) PSB, and (c, f) PSC surfactant. The films were heated at 350 °C for 10 min and at 500 °C for 1 min.

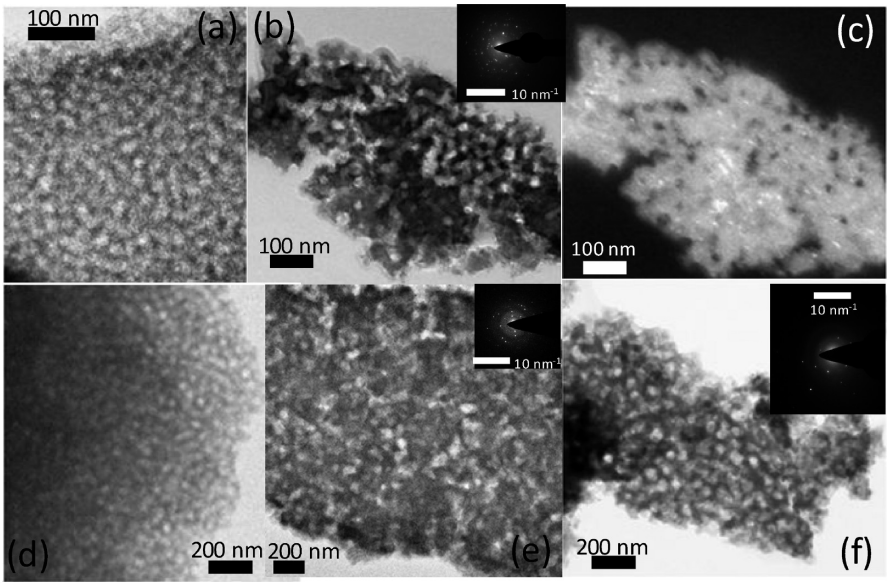

Figure 2. (a, b) Bright field TEM micrographs of $NbVO_5$ PSA films. The films were calcined at a rate of 10 °C/min up to 435 °C (a) and to 445 °C (b). (c) Dark field image of part b. (d, e) Bright field TEM micrographs of $NbVO_5$ PSB films calcined at a rate of 10 °C/min up to 455 °C (d) and 465 °C (e). (f) Bright field TEM micrograph of a PSB film calcined at 500 °C (60 s)−510 °C (30 s)−520 °C (30 s)−530 °C (30 s). Insets show the corresponding diffraction patterns.

dx.doi.org/10.1021/cm103481n |*Chem. Mater.* 2011, 23, 4124–4131

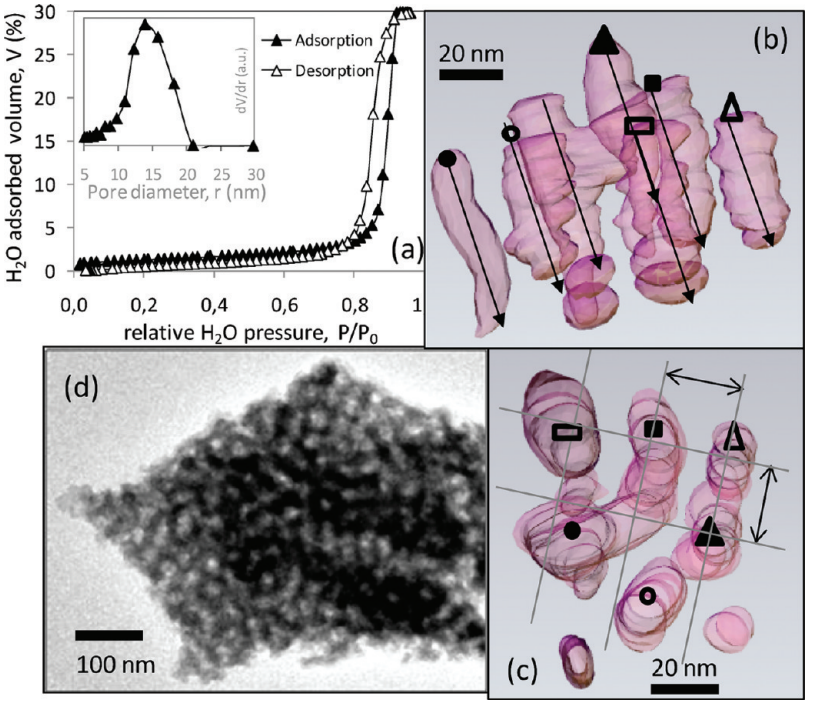

Figure 4. (a) Environmental ellipsometric porosimetry: water adsorption−desorption isotherm (main figure) and the corresponding pore-size distribution (inset) of a PSA-based $NbVO_5$ film treated at 500 °C for 1 min. (b, c) Electron tomography reconstruction: pores perpendicular to the substrate: side view (b); top view (c). (d) Corresponding TEM image at 0° tilt.

Porosimetric ellipsometric measurements are presented in Figure 4a for the PSA-film. The adsorption−desorption isotherm shows 30% water-accessible porous volume. The pore diameter distribution is centered on 14 nm (inset of Figure 4a), which is consistent with the size provided by TEM. The shape of the isotherm, characterized by the absence of hysteresis, suggests that the pores are shaped as closed cylinders.[36] In order to support this hypothesis, the film architecture has been visualized by electron tomography. The volume reconstructed from TEM images of the sample tilted around an axis is presented in Movie 1 of the Supporting Information; one of these TEM images is presented in Figure 4d. The movie shows the tridimensional mesoporous architecture. A portion of the reconstructed volume is presented in Figure 4b and c. It appears that pores have merged to form parallel tubes as predicted by the porosimetry measurement. The center to center distance was evaluated to be about 20 nm (Figure 4c). Two of these tubes are locally connected through a perpendicular channel which displays the tridimensionality of the mesoporous framework.

At this stage, the mesoporous Nb−V mixed oxide is amorphous. The achievement of a crystalline mesoporous film appears challenging because the diffusive sintering upon $NbVO_5$ crystalline growth is strongly detrimental to the mesostructure. In order to take up this challenge, films presenting thick inorganic walls (PSB-based) which are able to better accommodate sintering are investigated, and a careful thermal post-treatment allowing increase of the number of nucleation centers while limiting crystal growth was selected. The latter consists in a succession of very short flashes at high temperature, typically 500 °C (60 s)−510 °C (30 s)−520 °C (30 s)−530 °C (30 s), which was applied after the 350 °C (10 min) step on a PSB-based film. TEM and the corresponding diffraction pattern attest respectively of the preservation of the mesostructure and of the presence of $NbVO_5$ crystallites inside the walls (Figure 2f). In light of these results, it appears that only partial crystallization is possible and requires a delicate procedure. Therefore, it would be more convenient to use amorphous $NbVO_5$ for our electrochemical study of the stability of the MTF architecture. It is necessary to check that vanadium is found as V^{5+} in tetrahedral coordination in the amorphous phase just below the crystallization limit.

Electron paramagnetic resonance reveals the presence of V^{4+} in the films (Figure S.I.4A of the Supporting Information). More quantitative information concerning the surface of the film was obtained by X-ray photoelectron spectroscopy: 95% of the surface vanadium species are present as V^{5+}, while only 5% as V^{4+} was detected (Figure S.I.4B of the Supporting Information). The content of V^{4+} is small compared to what was reported in the literature for hybrid mesostructured thin films of pure vanadium oxide prepared by EISA.[21] The latter study pointed out that at least 50% of V^{4+} is needed, since it acts both as a condensation activator and as a 3D-orientator of the inorganic network to allow for pore curvature.[21] This V^{4+} property is actually widely used in the synthesis of vanadium oxide nanotubes.[37] In our case, Nb^{5+} appears to have a stabilizing effect on the inorganic network, allowing a lower V^{4+} content. Static ^{51}V solid state NMR experiments on scratched amorphous $NbVO_5$ MTFs heated at 500 °C for 1 min (see Figure S.I.4C of the Supporting Information) show the presence of vanadium with a chemical shift typical of tetrahedral coordination. The above results thus confirm that amorphous $NbVO_5$ films heated just below the crystallization limit contain mainly V^{5+} in coordination 4 and are therefore suitable for the electrochemical study.

Cyclic voltammograms of PSA, PSB, and PSC-$NbVO_5$ amorphous MTFs treated for 10 min at 500 °C are presented in Figure 5a. These curves are compared to the electrochemical response of a nonporous film as a reference.

dx.doi.org/10.1021/cm103481n |*Chem. Mater.* 2011, 23, 4124–4131

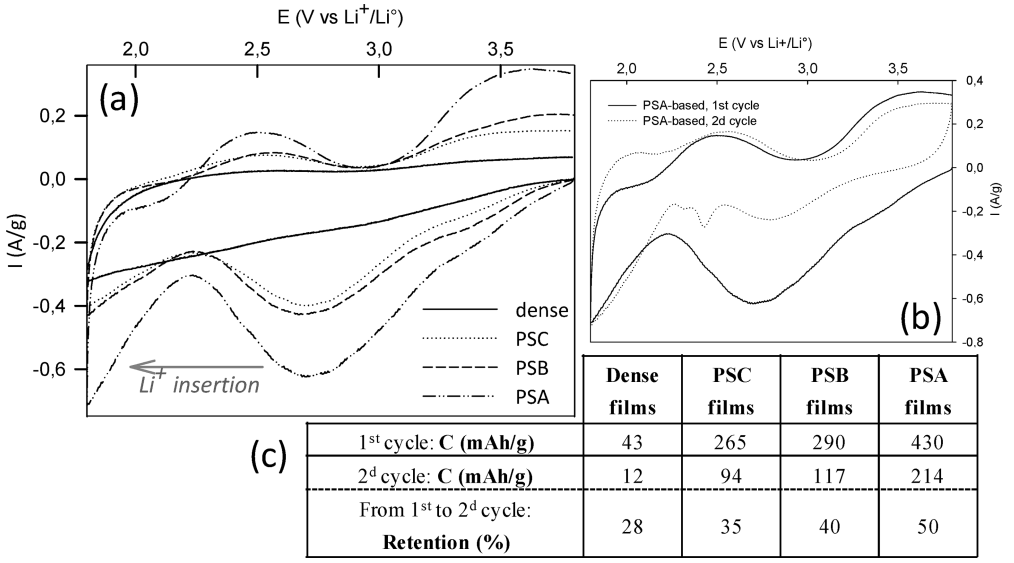

(c)

	Dense films	PSC films	PSB films	PSA films
1st cycle: **C (mAh/g)**	43	265	290	430
2d cycle: **C (mAh/g)**	12	94	117	214
From 1st to 2d cycle: **Retention (%)**	28	35	40	50

Figure 5. (a, b) Cyclic voltammograms obtained at a scan rate of 0.5 mV/s. (a) First cycles of PSA, PSB, PSC, and dense films of amorphous $NbVO_5$ heated at 500 °C. (b) First and second cycles of PSA films of amorphous $NbVO_5$ (heated at 500 °C). (c) Table reporting Li^+ insertion capacities of the first and second cycles for PSA, PSB, PSC, and dense films.

Regarding the capacity of the material to insert Li^+ during the first cycle, it appears that the current densities are larger for mesoporous films compared to dense films, confirming our preliminary results obtained for the PSA films.[24] The capacity is found to increase when the pore size decreases, i.e., from PSC to PSA. The PSA film, presenting the smallest pore size (~15 nm), is expected to present the highest capacity, due to the higher contact surface area between the electrode and the electrolyte.[34]

It is observed that the Li^+ inserted upon the first reduction process is not fully extracted during the first oxidation step (Figure 5a). In the case of the PSA film, for example, 1.3 Li^+ per $NbVO_5$ are inserted while only 0.5 Li^+ are effectively extracted (Figure 5b, c), neglecting the double layer/pseudocapacitive contribution and thus assuming that the totality of the current is assigned to the lithium insertion process (see Figure S.I.6 of the Supporting Information).

For the second cycle, the system presents more reversible lithium insertion/extraction (+0.8 Li^+/−0.5 Li^+). In addition, the integrity of the mesoporous architecture after 20 cycles was verified by TEM in the case of an amorphous PSA film (see Figure S.I.5 of the Supporting Information).

Poor reversibility in the first cycle is often attributed to the formation of a solid electrolyte interface (SEI) layer.[38] However, for V_2O_5 and Nb_2O_5 thin films prepared under similar conditions, this irreversibility is not observed.[24] SEI layer formation is therefore probably not the only relevant phenomenon. As mentioned in the Introduction, bulk crystalline $NbVO_5$ is known to lose 90% of its initial capacity after the first Li^+ insertion.[15,16] This value is close to what is obtained here for the dense amorphous film. The table in Figure 5c shows that the percentage of retained capacity from the first to the second cycle increases from PSC to PSA. Considering that capacity retention is directly related to the ability to accommodate mechanical stresses, our results suggest that better accommodation is obtained for smaller pore size and wall thickness (ratio of pore size and wall thickness is always ~1 in the present study). PSA films have pores in the 15 nm range.

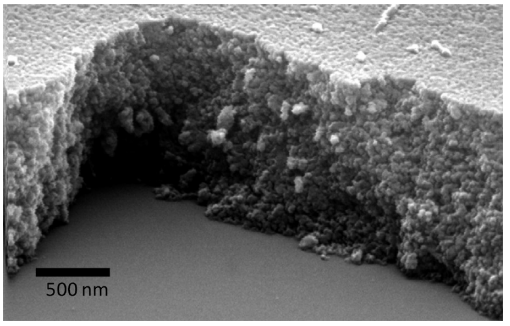

Figure 6. SEM micrograph of an amorphous $NbVO_5$ PSA thick film resulting from a multidipping process. The 1.3-μm-thick film on silicon consists of nine layers, stabilized at 180 °C after each layer deposition and finally heated at 350 °C for 5 h.

Increasing the capacity of the material may be achieved by increasing the film thickness through multilayer deposition. In the approach detailed in the Experimental Section, we take advantage of the high thermal stability of the PS-*b*-PEO structuring agent, rationally selecting the heat treatment applied between each deposition step in order to allow the condensation of the inorganic network to occur while keeping the structuring agent intact. After a final heat treatment at 500 °C, crack-free mesoporous thick films are obtained. Figure 6 shows the SEM micrograph of a 1.3-μm-thick PSA-$NbVO_5$ MTF prepared by multidipping (nine layers).

Ellipsometric porosimetry measurements reveal that the accessible porosity represents 17% of the bulk volume, compared to 30% for the 100-nm-thick one-layer film. This decrease is probably due to the numerous intermediate heat treatments. It might be possible to increase the accessible porosity through an optimization of the multilayer deposition, for example by applying the procedure recently described in ref 39. The cyclic voltammograms of multilayer films with up to nine layers are presented in Figure 7. It shows that the first cycle capacity regularly increases with the film thickness, proving that the

dx.doi.org/10.1021/cm103481n |*Chem. Mater.* 2011, 23, 4124–4131

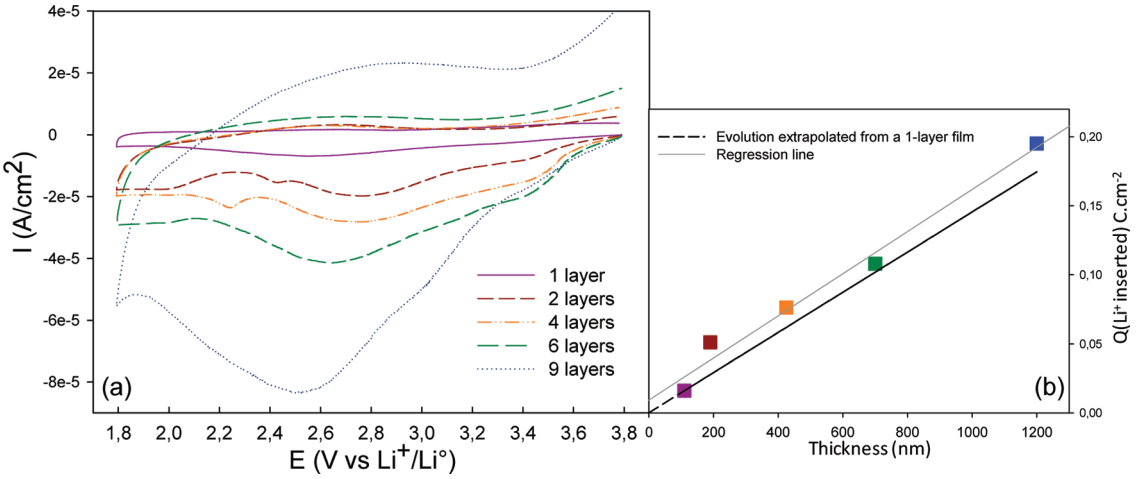

Figure 7. (a) Cyclic voltammograms (scan rate: 0.5 mV/s) of PSA-multilayer films. (b) Evolution of the current density of the reduction process as a function of the film thickness. The regression line is close to what could be expected from the extrapolated curve obtained from the value of a one-layer film.

interconnected porosity is effectively accessible to the electrolyte through the whole thickness of the film. The here-proposed multilayered process therefore appears promising for obtainment of thick mesoporous films. Since this process has been developed for a very complex system, it should be easily extended to a large range of materials used in energy storage applications.

4. CONCLUSION

This study uses in situ thermal ellipsometric analysis to better understand the limitations of synthesizing fully crystalline mixed oxide mesoporous thin films (MTFs) through the soft templating method. In the context of using mesoporous films in energy storage applications, this work highlights how small pores can be beneficial in terms of mechanical stability in the case of large structural distortion such as induced by lithium insertion in the $NbVO_5$ structure.

Amorphous $NbVO_5$ MTFs presenting wormlike mesoporous structure with pore and inorganic wall sizes from 15 to 100 nm were successfully obtained via the EIMP method from ethoxychloride precursor solutions containing micelles of PS-*b*-PEO structuring agent. Thermal ellipsometric analysis (TEA) performed on the stabilized films revealed the behavior of the mesoporous layer upon heating in terms of surfactant removal and crystallization. We found that the calcination of the structuring agent begins at about 220 °C with the PEO elimination and ends at around 380 °C with the PS micelle core removal. This confirmed the greater thermal stability of PS-*b*-PEO compared with Pluronic surfactants. Condensation reactions occurring at higher temperatures can consequently take place in the presence of the template. This mechanically stabilized framework can then support the complete removal of surfactant, leading to the mesoporous amorphous thin films shown here by AFM and TEM. Upon crystallization, however, TEA showed that this architecture undergoes an abrupt collapse as a result of the rapid diffusive sintering of the $NbVO_5$ crystallites. Only a fine control of the heat treatment together with thick inorganic walls ($\geq$50 nm) allows preserving the mesostructure while partially crystallizing the $NbVO_5$ phase, showing the limitations of the self-assembling method in obtaining a fully crystalline mixed oxide.

Lithium insertion in amorphous $NbVO_5$ MTFs with three different pore sizes was investigated by cyclic voltammetry and compared to the cases of nonporous films. It turned out that the mesoporous network was less drastically affected than the nonporous one by the structural modification. Furthermore, the smaller the MTF pore size, the higher its ability to accommodate stresses. In addition, the electrochemical characterizations confirmed the expected capacity gains offered by MTF architectures compared to nonporous thin films, due to the higher surface area in contact with the electrolyte. The capacity of the material could be increased by using thicker films prepared by the here proposed multilayer deposition (1.3-μm-thick films after nine layers).

■ ASSOCIATED CONTENT

Supporting Information. Figure S.I.1 presents the diffusion light scattering results for the PSA-, PSB-, and PSC-precursor solutions with and without inorganic precursors. Figure S.I.2 shows the thermal ellipsometry analyses collected for $NbVO_5$ PSA-films but also for PSB- and PSC-films. Figure S.I.3 presents X-ray diffractograms of the $NbVO_5$ PSB-films treated for 10 min at 350 °C (amorphous) and up to 600 °C (crystalline). Figure S.I.4 evaluates the oxidation state (using EPR and XPS results) and coordination (^{51}V static NMR) of vanadium in PSA-$NbVO_5$ film heated at 500 °C for 1 min. Figure S.I.5 shows the TEM image of $NbVO_5$ PSA-MTF after 20 cycles of Li^+ insertion−extraction (0.5 mV/s), highlighting the intact wormlike mesostructure. Figure S.I.6 presents a description of a typical PSA-$NbVO_5$ film voltammogram in terms of vanadium and niobium contributions; it also identifies one of the electrochemical processes occurring as a faradaic lithium diffusion controlled Process.[40,41] Movie 1 presents a visualization of the mesoporous architecture of a PSA-based thin film of amorphous $NbVO_5$. This material is available free of charge via the Internet at http://pubs.acs.org.

■ AUTHOR INFORMATION

Corresponding Author

*E-mail: clement.sanchez@upmc.fr. Telephone: +33 (0)1 44 27 15 01. Fax: +33 (0)1 44 27 15 04.

■ ACKNOWLEDGMENT

The authors would like to thank Yan Ledu from the UPMC (France) for the EPR measurements and fit. N.K. thanks the F.R.S.-F.NRS (National Fund for Scientific Research) in Belgium for a research fellowship. R.D. thanks the FRIA for his grant. E.G.'s group thanks the F.R.S.-F.NRS for the funding of the XPS equipment. Part of this work was supported by the Belgian Science Policy (Belgian State) under the Interuniversity Attraction Poles program (INANOMAT-P6/17).

■ REFERENCES

(1) Orilall, M. C.; Wiesner, U. *Chem. Soc. Rev.* **2011**, *40*, 520–535.
(2) Brezesinski, T.; Wang, J.; Tolbert, S. H.; Dunn, B. *Nat. Mater.* **2010**, *9*, 146–151.
(3) Brezesinski, T.; Wang, J.; Polleux, J.; Dunn, B.; Tolbert, S. H. *J. Am. Chem. Soc.* **2009**, *131*, 1802–1809.
(4) Lee, J.; Jung, Y. S.; Warren, S. C.; Kamperman, M.; Oh, S. M.; DiSalvo, F. J.; Wiesner, U. *Macromol. Chem. Phys.* **2011**, *222*, 383–390.
(5) Brezesinski, T.; Wang, J.; Haetge, J.; Reitz, C.; Steinmueller, S. O.; Tolbert, S. H.; Smarsly, B. M.; Dunn, B.; Brezesinski, T. *J. Am. Chem. Soc.* **2010**, *132*, 6982–6990.
(6) Szeifert, J. M.; Feckl, J. M.; Fattakhova-Rohlfing, D.; Liu, Y.; Kalousek, V.; Rathousky, J.; Bein, T. *J. Am. Chem. Soc.* **2010**, *132*, 12605–12611.
(7) Bruce, P. G.; Scrosati, B.; Tarascon, J.-M. *Angew. Chem., Int. Ed.* **2008**, *47*, 2930–2946.
(8) Centi, G.; Perathoner, S. *Eur. J. Inorg. Chem.* **2009**, 3851–3878.
(9) Cheng, F.; Tao, Z.; Liang, J.; Chen, J. *Chem. Mater.* **2008**, *20*, 667–681.
(10) Bruce, P. G.; Scrosati, B.; Tarascon, J.-M. *Angew. Chem., Int. Ed.* **2008**, *47*, 2930–2946.
(11) Sanchez, C.; Boissière, C.; Grosso, D.; Laberty, C.; Nicole, L. *Chem. Mater.* **2008**, *20*, 682–737.
(12) Xie, Y.; Wu, C. *Dalton Trans.* **2007**, 5235–5240.
(13) Sallard, S.; Brezesinski, T.; Smarsly, B. M. *J. Phys. Chem. C* **2007**, *111*, 7200–7206.
(14) Amarilla, J. M.; Casal, B.; Ruiz-Hitzky, E. *J. Mater. Chem.* **1996**, *6*, 1005–1011.
(15) Amarilla, J. M.; Perez-Revenga, M. L.; Casal, B.; Ruiz-Hitzky, E. *Catal. Today* **2003**, *78*, 571–579.
(16) Brown, J. D.; Altermatt, D. *Acta Crystallogr., Sect. B: Struct. Sci.* **1985**, *41*, 244–247.
(17) Ren, Y.; Armstrong, A. R.; Jiao, F.; Bruce, P. G. *J. Am. Chem. Soc.* **2010**, *132*, 996–1004.
(18) Sayle, T. X. T.; Maphanga, R. R.; Ngoepe, P. E.; Sayle, D. C. *J. Am. Chem. Soc.* **2009**, *131*, 6161–6173.
(19) Yang, P.; Zhao, D.; Margolese, D. I.; Chmelka, B. F.; Stucky, G. D. *Chem. Mater.* **1999**, *11*, 2813–2826.
(20) Brezesinski, T.; Groenewolt, M.; Pinna, N.; Amenitsch, H.; Antonietti, M.; Smarsly, B. *Adv. Mater.* **2006**, *18*, 1827–1831.
(21) Crepaldi, E. L.; Grosso, D.; Soler-illia, G. J. de A. A.; Albouy, P.-A.; Amenitsch, H.; Curie, M. *Chem. Mater.* **2002**, 3316–3325.
(22) Wu, C.; Wei, H.; Ning, B.; Xie, Y. *Adv. Mater.* **2010**, *22*, 1–5.
(23) Yuan, L.; Bhatt, S.; Beaucage, G.; Guliants, V. V.; Mamedov, S.; Soman, R. S. *J. Phys. Chem. B* **2005**, *109*, 23250–23254.
(24) Krins, N.; Lepot, L.; Cloots, R.; Vertruyen, B. *Solid State Ionics* **2009**, *180*, 848–852.
(25) Yu, K.; Hurd, A. J.; Eisenberg, A.; Brinker, C. J. *Langmuir* **2001**, *17*, 7961–7965.
(26) Kuemmel, M.; Allouche, J.; Nicole, L.; Boissière, C.; Laberty, C.; Amenitsch, H.; Sanchez, C.; Grosso, D. *Chem. Mater.* **2007**, *19*, 3717–3725.
(27) Sassoye, C.; Laberty, C.; Le Khanh, H.; Cassaignon, S.; Boissière, C.; Antonietti, M.; Sanchez, C. *Adv. Funct. Mater.* **2009**, *19*, 1922–1929.
(28) Boissiere, C.; Grosso, D.; Lepoutre, S.; Nicole, L.; Bruneau, A. B.; Sanchez, C. *Langmuir* **2005**, *21*, 12362–71.
(29) Bass, J. D.; Grosso, D.; Boissiere, C.; Sanchez, C. *J. Am. Chem. Soc.* **2008**, *130*, 7882–97.
(30) Stoll, S.; Schweiger, A. *J. Magn. Reson.* **2006**, *178*, 42–55.
(31) Benayad, A.; Martinez, H.; Gies, A.; Pecquenard, B.; Levasseur, A.; Gonbeau, D. *J. Electron Spectrosc. Relat. Phenom.* **2006**, *150*, 1–10.
(32) Crepaldi, E. L.; Soler-Illia, G. J. de A. A.; Grosso, D.; Cagnol, F.; Ribot, F.; Sanchez, C. *J. Am. Chem. Soc.* **2003**, *125*, 9770–9786.
(33) Bass, J. D.; Grosso, D.; Boissiere, C.; Sanchez, C. *J. Am. Chem. Soc.* **2008**, *130*, 7882–7897.
(34) Brezesinski, T.; Rohlfing, D. F.; Sallard, S.; Antonietti, M.; Smarsly, B. M. *Small* **2006**, *10*, 1203–1211.
(35) Huguenin, F.; Torresi, R. M.; Buttry, D. A.; Pereira Da Silva, J. E.; Cordoba de Toresi, S. *Electrochim. Acta* **2001**, *46*, 3555–3562.
(36) Rouquerol, F.; Rouquerol, J.; Sing, K. *Adsorption by Powders and Porous Solids—Principles, Methodology and Applications*; Academic Press: London, 1998.
(37) Nordlinder, S.; Nyholm, L.; Gustafsson, T.; Edström, K. *Chem. Mater.* **2006**, *18*, 495–503.
(38) Swiatowskamrowiecka, J.; Maurice, V.; Zanna, S.; Klein, L.; Briand, E.; Vickridge, I.; Marcus, P. *J. Power Sources* **2007**, *170*, 160–172.
(39) Krins, N.; Faustini, M.; Louis, B.; Grosso, D. *Chem. Mater.* 2010, 101112095318045.
(40) Desportes, C.; Duclot, M.; Fabry, P.; Fouletier, J.; Hammou, A.; Kleitz, M.; Siebert, E. *Electrochimie des solides*; Science Collection Grenoble; 2000; 440 pp.
(41) Xie, J.; Imanishi, N.; Hirano, A.; Matsumura, M.; Takeda, Y.; Yamamoto, O. *Solid State Ionics* **2007**, *178*, 1218–1224.